

Article

Research on Gas Control Technology in Goaf Based on the Influence of Mining Speed

Cheng Cheng ^{1,2,*}, Xiao-Yu Cheng ¹, Long Chen ¹ and Xing-Ying Ma ¹

¹ China Coal Energy Research Institute Co., Ltd., Xi'an 710054, China; chengxiaoyu@chinacoal.com (X.-Y.C.); chenlong1@chinacoal.com (L.C.); mxy6629@123.com (X.-Y.M.)

² College of Safety Science and Engineering, Xi'an University of Science and Technology, Xi'an 710054, China

* Correspondence: 18717314036@163.com

Abstract: To comprehensively understand the influence of mining speed on gas emissions in goaf during coal seam extraction, enhance gas extraction efficiency in goaf, manage gas emissions at the working face, and ensure safety in the mining production process. This study focuses on the No. 3 mining area of Wangjialing Mine, employing numerical simulations to analyze the evolution of mining-induced fractures and the characteristics of gas distribution in the overburden at varying mining speeds. Furthermore, by integrating actual gas emission and extraction data at the production face, this study examines the quantitative relationship between mining speed and gas emissions in the goaf, identifying optimal regions for high-position borehole layouts and conducting borehole optimization design and investigation. The results of this study indicate that the initial caving step distance of the goaf roof increases with the advancement speed of the working face. Conversely, the maximum height of through fractures in the overburden decreases as the mining speed increases, while delamination fractures are minimally affected by the advancement speed. By categorizing and averaging data on goaf mining speed, the impact of initial and periodic pressure on gas emissions can be effectively mitigated, revealing a linear correlation coefficient of 0.94 between goaf gas emissions and mining speed. At varying mining speeds of the working face, the efficient extraction layer and horizontal distance parameters of gas extraction boreholes in the goaf conform to the linear equation $y = ax \pm b$. Based on the research findings, an optimization design for mining face speed and high-level borehole parameters in the goaf was implemented. The average gas extraction rate of high-level directional boreholes reached 68% throughout the extraction period. Gas emissions at the working face were effectively controlled below $10 \text{ m}^3/\text{min}$, with the maximum gas concentration at the upper corners and return airflow kept below 0.8%. This effectively managed gas emissions at the working face, ensuring safe production in the mine, providing a theoretical basis for identifying gas-rich areas in the mining-induced overburden, and enhancing gas extraction efficiency at the working face.

Keywords: mining-induced fractures; mining speed; numerical simulation; gas extraction; high-level borehole optimization



Citation: Cheng, C.; Cheng, X.-Y.; Chen, L.; Ma, X.-Y. Research on Gas Control Technology in Goaf Based on the Influence of Mining Speed. *Processes* **2024**, *12*, 1528. <https://doi.org/10.3390/pr12071528>

Academic Editor: Guining Lu

Received: 28 June 2024

Revised: 16 July 2024

Accepted: 18 July 2024

Published: 20 July 2024



Copyright: © 2024 by the authors. Licensee MDPI, Basel, Switzerland. This article is an open access article distributed under the terms and conditions of the Creative Commons Attribution (CC BY) license (<https://creativecommons.org/licenses/by/4.0/>).

1. Introduction

Coal serves as the “ballast stone” of China’s energy security, and ensuring the safe and efficient extraction of coal mines is crucial for maintaining this security [1,2]. As the number of ten-million-ton mines in the country increases, the mining intensity of coal mines also rises. Due to high-intensity mining at the working face, gas emissions in mines escalate, making gas disasters a key factor restricting the safe production of coal mines [3–5]. Especially during high-intensity mining at the working face, gas emissions in the goaf increase sharply, causing gas over-limit at the coal mining face, upper corners, and return airflow, thereby posing significant safety hazards to the mine [6,7]. Therefore, to effectively carry out gas prevention and control in the goaf, it is first necessary to determine the emission and accumulation characteristics of gas in the goaf, enabling the implementation

of targeted measures. However, during mine production, the gas emission and migration characteristics in the goaf are influenced by the advancement speed of the working face. The collapse and fracture development of the mining-induced overburden in the goaf exhibit significant variations, complicating the accurate determination of gas-rich locations within the fracture zone. This results in inefficiencies in extracting gas from the fractures of the overburden through high-level directional long boreholes in the goaf [8]. Therefore, it is imperative to study the evolution of fractures in the overburden influenced by the mining face speed and the gas emission characteristics in the goaf to enhance the gas management capacity of the mine goaf.

Numerous scholars have extensively studied the characteristics of gas emission and migration in the goaf. Empirical evidence has shown that the main sources of gas in the goaf are residual coal, air leakage at the working face, and gas migration from adjacent strata. After being emitted, the gas migrates and accumulates in the fracture zones of the overburden in the goaf [9–13]. Therefore, examining the development characteristics of mining-induced overburden fractures can effectively elucidate the gas migration patterns in the goaf. Qian Minggao, Yuan Liang, Li Shugang, and others have proposed various theories on mining field movement, including the “O-ring”, “high-position annular body”, “vertical three zones”, and “elliptic parabolic zone” theories [14–16]. Building upon these theories, numerous scholars have further explored the evolution characteristics of overburden fractures in the goaf using methods such as numerical simulation, physical simulation, and field experiments. Islam [17] and Wu [18] employed numerical simulations to investigate the characteristics of overburden collapse during working face mining and analyzed the fracture zone development process. Lin [19] utilized physical similarity simulation methods to experimentally analyze the dynamic evolution process of overburden fractures during coal seam mining. Zhang [20] and Kang [21] respectively utilized peeping technology and borehole water injection experiments to analyze the development characteristics of the mining-induced fracture zone in the overburden on site. Yuan [22] and colleagues employed electromagnetic methods to conduct on-site testing and analysis of overburden fractures during coal seam mining based on the electrical characteristics of the overburden fractures. Zhang [23] conducted a comprehensive study on the evolution characteristics of overburden fractures in fully mechanized mining using a combination of theoretical analysis, numerical simulations, and field measurements. Concurrently, numerous scholars have studied the migration and distribution patterns of gas in the goaf based on research on mining-induced overburden fractures, providing fundamental theoretical support for gas management in the goaf. Zhou [24] and Qin [25] employed numerical simulations to analyze the gas migration characteristics within mining-induced fractures, obtaining the flow characteristics of gas in the annular high-permeability zones of the overburden under different working conditions. Guo [26] and colleagues utilized finite element simulations to analyze the dynamic interaction between stress, overburden fractures, and gas seepage during working face mining. Zhang [27] employed physical experiments to investigate the permeability evolution characteristics of fractured coal under different pressures, analyzing the gas seepage and migration patterns in the compaction and fracture zones of the goaf. Liu [28] and colleagues examined the migration and distribution characteristics of gas within overburden fracture zones under gas extraction conditions in the goaf.

The aforementioned research results have significantly advanced the understanding of mining-induced overburden fractures and gas accumulation characteristics in the goaf, and substantial progress has been made in gas management within the goaf. However, research on the characteristics of gas emission and distribution in the goaf considering the impact of the working face advancement speed has been limited. Additionally, there has been scant research on the gas accumulation characteristics in the mining-induced overburden fracture zone affected by the advancement speed, thereby limiting the guidance for on-site gas management. Therefore, it is imperative to further study the evolution of mining-induced overburden fractures and the characteristics of gas emission in the goaf under the influence of the mining speed. This will effectively guide the selection of areas

for high-level directional long borehole placement in the goaf and enhance the effectiveness of gas management in the mine goaf.

This paper employs numerical simulations to investigate the evolution of the fracture zone distribution range in the overburden layers of the goaf under varying mining speeds. It identifies the characteristics of gas accumulation in the goaf as influenced by the mining speed. Based on field measurement data, it analyzes the gas emission patterns in the goaf and quantifies the relationship between the optimal borehole layer and horizontal distance affected by the mining speed. According to the research results, it optimizes the parameters of high-level boreholes in the goaf and conducts field tests. The research findings provide theoretical support for identifying gas accumulation zones in mining-induced overburden and for optimizing high-level boreholes.

2. Evolution Characteristics of Mining-Induced Fractures and Gas Migration Patterns Affected by Mining Speed

2.1. Overview of Engineering Conditions in the Test Area and Establishment of the Numerical Model

Wangjialing Coal Mine, situated in Xiangning County, Shanxi Province, encompasses a mining field area of 119.7 km². The mine utilizes primary and auxiliary inclined shafts for development and employs the longwall retreat mining method combined with fully mechanized top coal caving technology. It is a quintessential high-production, high-efficiency coal mine characterized by high gas emissions at the working face.

The selected test area is the third mining area of Wangjialing Coal Mine, characterized by an average coal thickness of 6 m and a simple coal seam structure. During the production process at the working face, gas emissions from the goaf constitute 45.5% of the total gas emissions at the working face. Gas in the goaf is primarily extracted using high-level directional long boreholes and buried pipes. However, during the mining process, due to a high mining intensity and inadequately matched borehole design parameters and construction, the gas extraction efficiency at the working face is suboptimal, leading to elevated gas concentration hazards in the return air corner. Therefore, determining an optimal working face mining speed and enhancing the gas extraction rate at the working face are critical issues that require urgent resolution in the mine.

UDEC 3.0 is a two-dimensional discrete element numerical calculation program for discontinuous medium models, typically used to solve engineering problems involving discontinuous rock masses, and it performs well in representing large discontinuous deformations in jointed rock masses. For the mechanical characteristics of discontinuous media under load, it can accurately simulate the joint and layer collapse processes of rock masses. Therefore, in this paper, UDEC 3.0 numerical simulation software was used to establish the numerical calculation model shown in Figure 1, simulating the evolution of mining-induced overlying rock fractures at mining speeds randomly set at 0–4 m/d, 4–8 m/d, and 8–12 m/d.

The values assigned to the strata at each level in the model are derived from the geological conditions and the physical–mechanical properties of the coal seam located in the No. 3 mining area of Wangjialing Coal Mine. The specific parameters are detailed in Table 1. The model dimensions are (XY): 500 × 420 m. A 100 m boundary protection coal pillar is left at each end of the model to mitigate the boundary effects of mining. The mining depth of the coal seam is 508.5 m. The weighted average bulk density of the overburden is 23.3 kN/m³, resulting in an overburden pressure of 23.3 kN/m³ × 508.5 m = 11.85 MPa. The lateral pressure coefficient is set at 1, resulting in a lateral pressure of 11.85 MPa × 1 = 11.85 MPa. The model's boundary conditions are defined as follows: zero displacement is imposed on the bottom, left, and right boundaries, whereas the upper boundary is free. The “Mohr–Coulomb” slip model is utilized for coal-rock damage, while the Coulomb slip model is employed for joints and fractures. Joints are divided in the horizontal and vertical directions within the model to simulate the distribution of joints in real rock strata, with a gravitational acceleration of 9.8 m/s². During the experiment, stepwise excavation is conducted along the strike, with a cycle progress of 0.80 m, totaling 279.6 m of excavation.

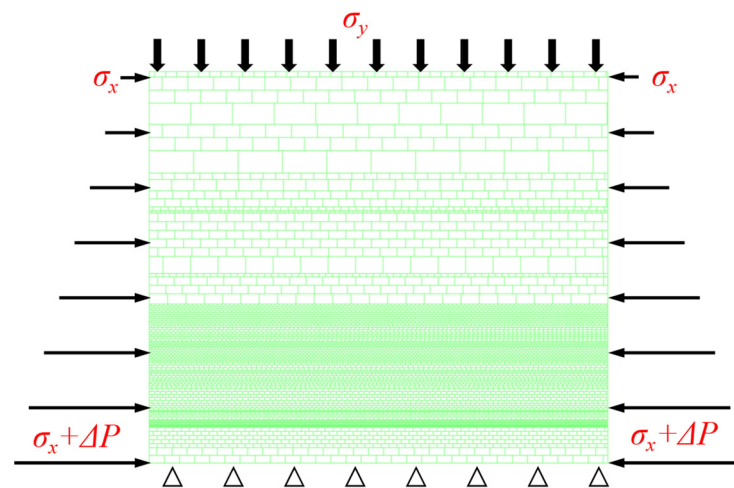


Figure 1. Numerical simulation model.

Table 1. Physical and mechanical parameters of coal and rock strata.

Lithology	Strata Thickness (m)	Elastic Modulus (GPa)	Angle of Internal Friction (°)	Tensile Strength (MPa)	Density (kg·m ⁻³)
Loess	40.87	/	/	/	1800
Sandy mudstone	36	5.62	35	2.91	2635
Sandy mudstone	25.56	5.62	35	2.91	2635
Mudstone	21.7	4.35	33.5	2.88	2643
Siltstone	25.75	9.86	35	2.67	2660
Sandy mudstone	5.35	5.62	35	2.91	2635
Siltstone	55	9.86	35	2.67	2660
Sandy mudstone	27.4	5.62	35	2.91	2635
Sandy mudstone	18.4	5.62	35	2.91	2635
Siltstone	32.8	9.86	35	2.67	2660
Mudstone	3.15	4.35	33.5	2.88	2643
Siltstone	1.8	9.86	35	2.67	2660
Medium-grained sandstone	7.35	8.76	42	7.92	2652
Mudstone	17.85	4.35	33.5	2.88	2643
Sandy mudstone	33.42	5.62	35	2.91	2635
Fine-grained sandstone	22.85	7.86	32	2.98	2645
Sandy mudstone	16	5.62	35	2.91	2635
Fine-grained sandstone	7.25	7.86	32	2.98	2645
Sandy mudstone	2.5	5.62	35	2.91	2635
Fine-grained sandstone	7.4	7.86	32	2.98	2645
Sandy mudstone	2.5	5.62	35	2.91	2635
#2 Coal seam	5.69	2.37	24	0.18	1390
Siltstone	0.86	9.86	35	2.67	2660
Sandy mudstone	2.22	5.62	35	2.91	2635
#3 Coal seam	0.33	2.37	24	0.18	1390

2.2. Influence of Working Face Advancement Speed on the Evolution of Mining-Induced Fractures

Figure 2a–c illustrate the characteristics of direct roof fracture development under varying mining speeds. At a mining speed of 0–4 m/d, when the working face advances 19.6 m, the direct roof collapses into the goaf, with a fracture height of 7.16 m and a delamination fracture height of 20.73 m. At a mining speed of 4–8 m/d, the collapse step distance increases to 26.8 m, with a fracture height of 10.69 m and a delamination fracture height of 20.54 m. When the working face advances at a speed of 8–12 m/d and reaches 33.2 m, the direct roof initially collapses, with both the fracture and delamination fracture heights developing to 10.62 m. Compared to the 4–8 m/d advancement speed, the maximum fracture and delamination fracture heights remain consistent.

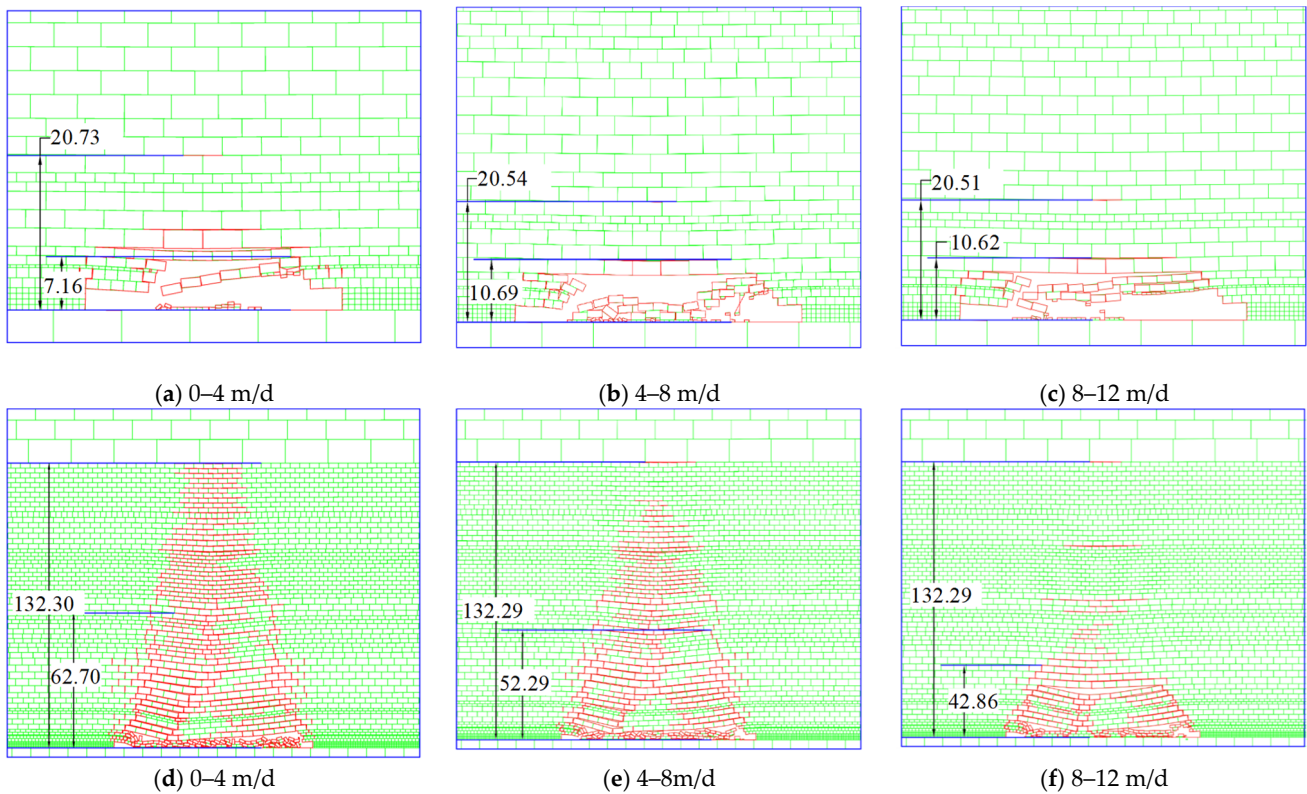


Figure 2. Effect of mining speed on the characteristics of mining-induced fractures in overlying strata.

Figure 2d–f depict the evolution characteristics of composite key layer fractures influenced by various mining speeds. During the mining process at varying speeds, mining-induced fractures continuously develop and close. The rock strata in the middle of the goaf gradually compact, forming a compaction zone, while a trapezoidal mining-induced fracture network forms on both sides of the goaf. After the third periodic pressure, the development height of the mining-induced overburden fractures gradually stabilizes. Influenced by varying mining speeds, there are significant differences in the final heights of through-going fractures after mining stabilizes. The maximum heights of through-going fractures are 62.70 m, 52.29 m, and 42.86 m at mining speeds of 0–4 m/d, 4–8 m/d, and 8–12 m/d, respectively.

Plot the maximum height curves of through-going fractures and delamination fractures at varying mining speeds, as depicted in Figure 3. The overall trend of through-going and delamination fracture development remains consistent across the three different advancement speeds. However, due to varying mining speeds, the initial collapse step distance of the direct roof varies, increasing with higher speeds. When the through-going fractures reach their maximum height, it is greatest at a mining speed of 0–4 m/d. As the mining speed increases, the maximum height of through-going fractures gradually decreases. This is due to the subsidence of the overlying soft rock and the mutual compression of adjacent strata, which cause the original fractures to close. Regarding delamination fractures, when the working face advances to the third periodic pressure, the delamination fractures stabilize at around 132 m and remain stable for an extended period. They start developing again when the working face advances to 175.6 m, with the development trend and height remaining highly consistent. The development of delamination fractures is generally less influenced by mining speed.

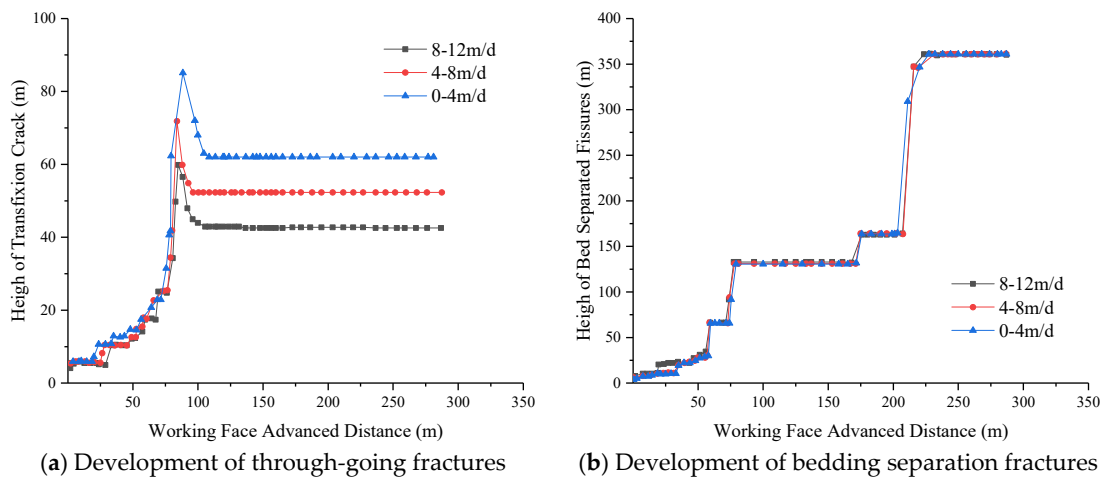


Figure 3. Maximum height curves of through-going fractures and separation fractures.

2.3. Gas Distribution Characteristics in Goaf Affected by Mining

The composition of gas sources in the fully mechanized caving face is illustrated in Figure 4, primarily comprising Q_1 gas emissions from caving coal, Q_2 gas emissions from the coal wall, and Q_3 gas emissions from the goaf. Among these, gas emissions from the goaf consist of emissions from residual coal and adjacent layers. Therefore, for gas emissions from the goaf in the fully mechanized caving face, factors such as the coal seam gas content and the volume of residual coal in the goaf significantly influence the emission situation. Additionally, given the extensive spatial range of the goaf and the substantial accumulation of gas, scenarios like the initial pressure of the main roof, periodic pressure, large-scale roof collapse, and goaf leakage can all induce substantial gas emissions from the goaf.

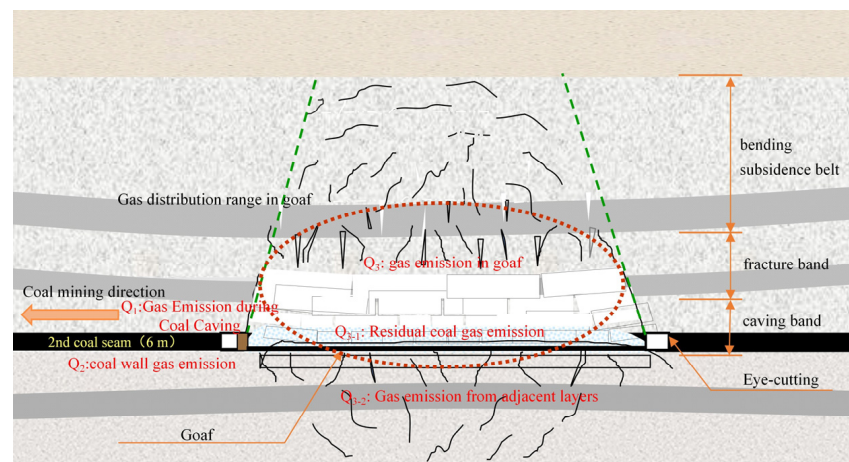


Figure 4. Composition diagram of gas sources in a fully mechanized caving mining face.

During the mining process at the working face, gas migration in the goaf can be divided into three main stages. The first stage involves gas release due to decompression, which rises upwards. The migration and storage areas of decompressed gas are primarily in the surrounding and top fracture zones of the overlying strata. The second stage occurs when decompressed gas in the top fracture zone becomes saturated, diffusing into the mining-induced fracture area and gradually filling the fracture and compaction zones. The rock strata in the compaction zone of the mining-induced fracture field become compacted, reducing porosity and hindering the migration of decompressed gas. At this stage, decompressed gas primarily migrates within the fracture zone of the fracture belt. The third stage involves emitted gas flowing through fractures into the deeper parts of the

goaf, merging with gas from residual caving coal, the coal wall, and adjacent working face coal seams, causing the gas concentration in the deeper goaf to gradually increase.

During the gas migration process of decompressed gas in the working face of Wangjialing Coal Mine's third mining area, as the working face advances, the gradual destruction of the immediate roof and the composite key layer in the goaf causes the gas to rise and accumulate in the fracture zone of the overlying strata. When the roof fracture stabilizes, part of the rock layer subsides, causing the original fractures and delamination cracks to close. Once the fractures close, their porosity sharply decreases. The cantilever of the overlying strata increases, and during rock layer breakage, newly formed fractures and delamination cracks become the main channels for decompressed gas migration. Although the porosity sharply decreases after the rock layer closes, gas can still migrate within, forming a complex mining-induced fracture network that permeates the entire fracture field. Decompressed gas gradually accumulates at the top of the fracture zone along the mining-induced fracture network. When decompressed gas in the top fracture zone reaches saturation, it gradually fills the entire mining-induced fracture field. Due to the gradual compaction of the central rock layer in the goaf, decompressed gas primarily migrates within the fracture zone. Additionally, with the continuous influx of fresh airflow, leakage airflow carries decompressed gas into the deeper parts of the goaf.

According to the numerical simulation results of mining-induced fracture evolution, the gas migration and distribution characteristics in the goaf at different advancing speeds are presented in Table 2.

Table 2. Gas accumulation height in the fully mechanized caving mining face.

Mining Speed m/d	Height of Gas Aggregation/m			
	Initial Weighting	Second Weighting	Third Weighting	Stope Stability
0–4	7.16	22.84 m	41.76	62.70
4–8	10.69	17.96	34.66	52.29
8–12	10.62	14.53	25.30	42.86

3. Influence of Mining Speed on Goaf Gas Emission and Accumulation Characteristics

3.1. Correlation Analysis Between Mining Speed and Goaf Gas Emission

To investigate the impact of the working face mining speed on gas emissions from the goaf, this study statistically analyzes historical data on gas emissions and mining speeds from the third mining area of Wangjialing Mine. The variation curves of gas emissions with the mining speed are plotted in Figures 5 and 6.

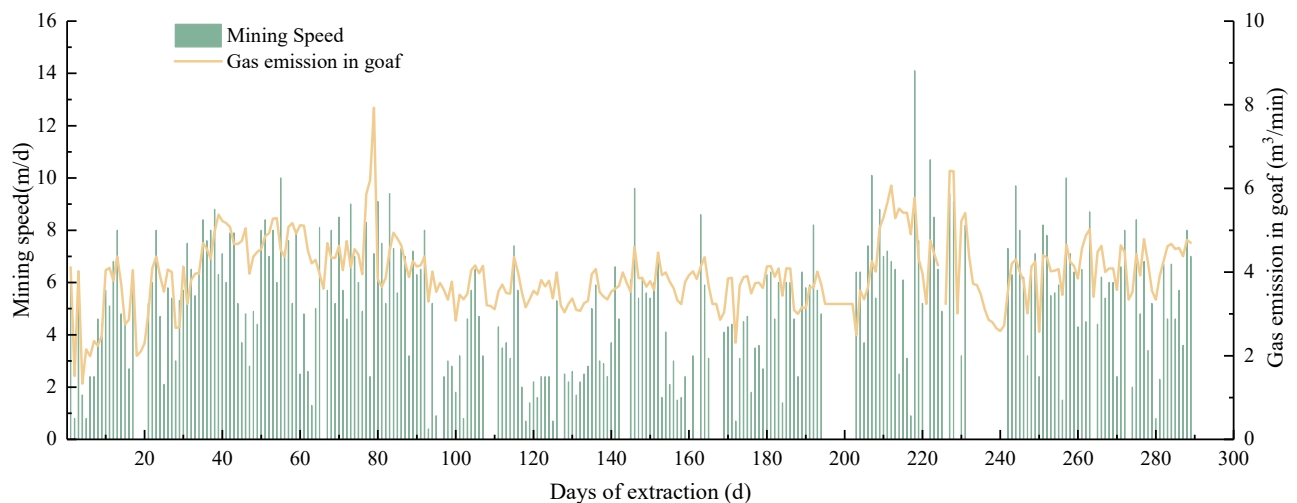


Figure 5. Evolution curve of goaf gas emission and mining speed.

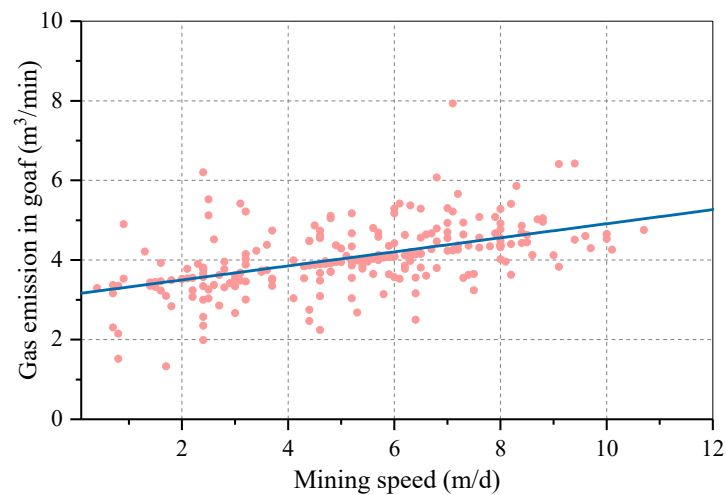


Figure 6. Correlation between goaf gas emission and mining speed.

To further elucidate the influence of mining speed on gas emissions and minimize the impact of confounding factors, the mining speed was categorized into stages at specific intervals. The average values of the mining speed and gas emissions within these intervals were calculated and are presented in Table 3, with a linear relationship plotted in Figure 7.

Table 3. Data statistics for speed interval classification.

Velocity Range (m·d ⁻¹)	Sample Size	Mining Speed (m·d ⁻¹)	Gas Emission Quantity (m ³ ·min ⁻¹)	Velocity Range (m·d ⁻¹)	Sample Size	Mining Speed (m·d ⁻¹)	Gas Emission Quantity (m ³ ·min ⁻¹)
0.0~0.5	40	0.01	3.22	5.6~6.0	28	5.83	4.16
0.6~1.0	9	0.79	3.07	6.1~6.5	23	6.34	4.13
1.1~1.5	5	1.42	3.55	6.6~7.0	13	6.83	4.62
1.6~2.0	9	1.76	3.16	7.1~7.5	14	7.26	4.57
2.1~2.5	22	2.36	3.62	7.6~8.0	17	7.91	4.58
2.6~3.0	12	2.82	3.50	8.1~8.5	10	8.32	4.63
3.1~3.5	13	3.23	3.97	8.6~9.0	5	8.78	4.66
3.6~4.0	6	3.67	3.88	9.1~9.5	4	9.25	5.29
4.1~4.5	12	4.34	3.75	9.6~10.0	4	9.83	4.52
4.6~5.0	21	4.73	4.01	>10.0	3	11.63	4.93
5.1~5.5	19	5.31	3.95	correlation coefficient		0.94	

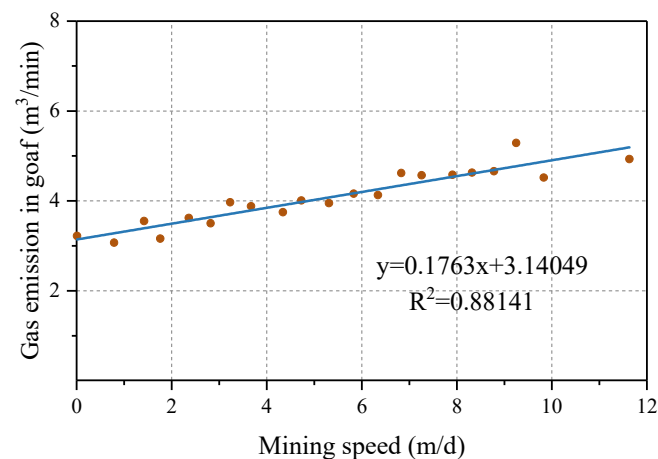


Figure 7. Linear relationship between mining speed and goaf gas emission.

After classifying and analyzing the mining speed, the correlation between the gas emissions from the goaf and the mining speed markedly increased from 0.60 to 0.94. This indicates that initial and periodic pressures during the mining process significantly impact gas emission volumes. Figure 7 presents the scatter plot and fitting curve of gas emissions from the goaf and the mining speed after data classification. The figure clearly shows that gas emissions from the goaf are influenced by the mining speed, exhibiting a linear relationship and indicating a strong correlation.

Due to the implementation of the fully mechanized top-coal caving method, residual coal remains in the goaf during mining, and gas from adjacent layers infiltrates the goaf through fracture channels. This results in significant gas accumulation in the goaf and fracture zone. Therefore, even at low mining speeds or during stoppage periods, gas emission volumes can still be maintained at a certain level. As gas emission attenuates over time, the emission capacity of residual coal at the same depth varies with different mining speeds. When the mining speed increases, the gas emission volume of residual coal correspondingly increases, exhibiting linear growth.

3.2. Optimal Zones for Gas Extraction Boreholes in Overburden Affected by Mining Speed

The mining speed of the working face significantly influences the collapse and fracture development of the overlying strata. The collapse and fracture development of the overlying strata vary with different mining speeds of the working face. Therefore, the optimal layer and horizontal distance of gas extraction boreholes in the goaf can be determined based on historical mining speeds.

Based on the recovery conditions of the mining face in the experimental mine, historical data on borehole design layers/horizontal distance and gas extraction volumes were collected for recovery speeds of 0–4 m/d, 4–8 m/d, and 8–12 m/d. The relationship between the gas extraction volume and layer/horizontal distance at different recovery speeds was then analyzed, as presented in the first and second columns of Table 4. The borehole layers and horizontal distance that exhibited better extraction effects at different recovery speeds were subsequently selected, and a scatter plot was drawn, as shown in the third column of Table 4. The relationship between the borehole layers and horizontal distance was fitted to obtain the quantitative relationship of the optimal layers and horizontal distance for extraction boreholes at different recovery speeds, as also shown in Table 5.

Table 4. Relationship between borehole extraction capacity and layer/horizontal distance at different mining speeds.

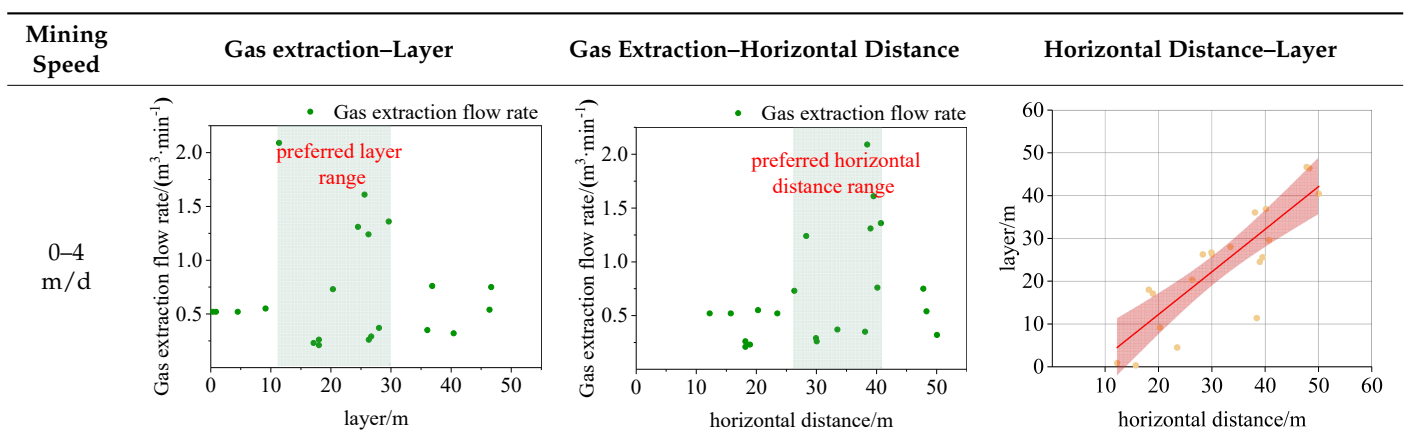


Table 4. Cont.

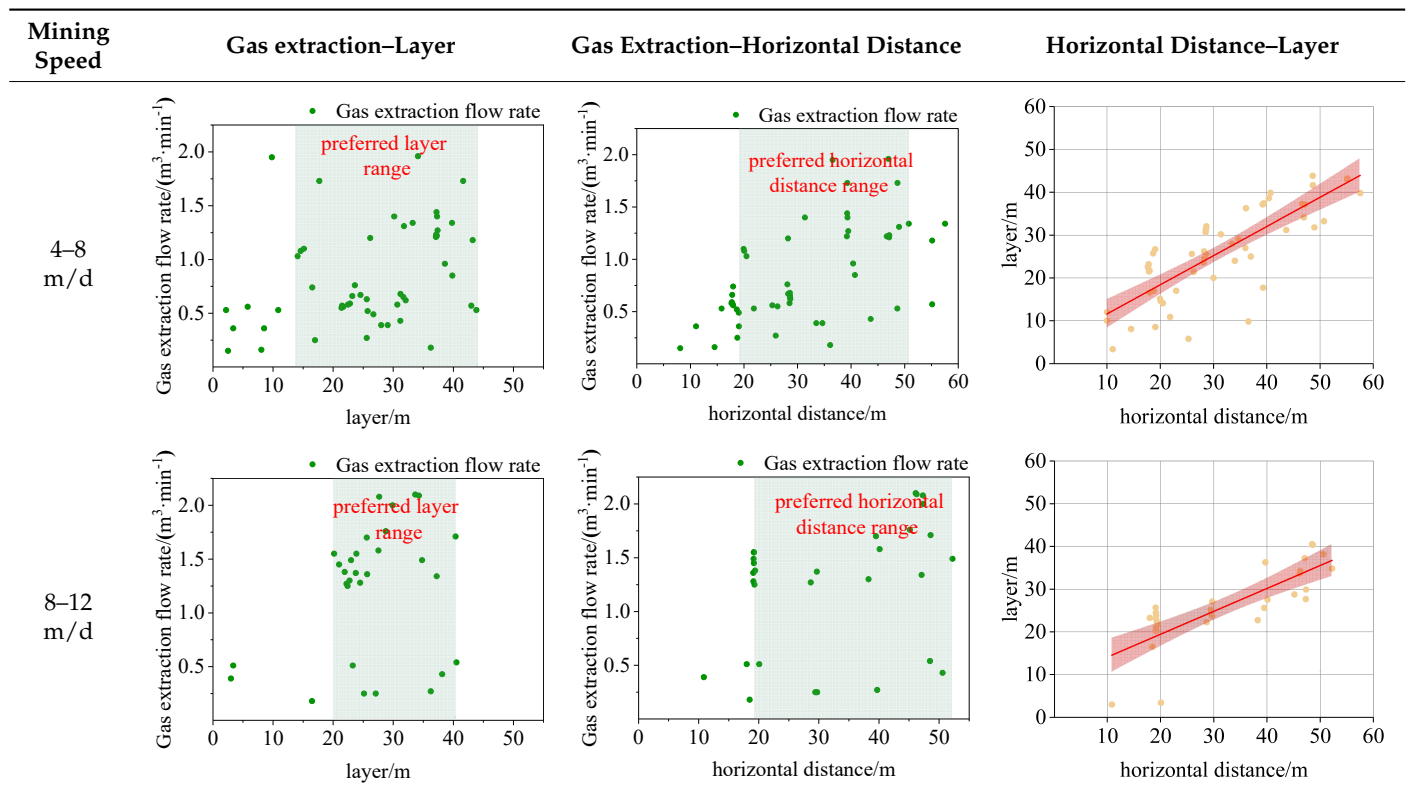


Table 5. Optimal borehole layer/horizontal distance for different mining speeds.

Mining Speed m/d	Preferred Layer /m	Preferred Horizontal Distance /m	Quantitative Relationship	R ²
0–4	12–30	26–41	$y = 0.9959x - 7.6928$	0.7152
4–8	14–44	17–51	$y = 0.8199x + 4.0584$	0.6461
8–12	21–41	21–52	$y = 0.5360x + 8.7194$	0.6354

Tables 4 and 5 illustrate that the optimal layer of boreholes with enhanced extraction effects vary with different mining speeds. Overall, as the mining speed of the working face increases, the optimal layer and horizontal distance of boreholes also increase. The optimal borehole layer and horizontal distance at different mining speeds fit a linear equation $y = ax \pm b$, with a good fit ($R^2 > 0.6$). Therefore, these quantitative relationships of the optimal borehole layer and horizontal distance under different mining speeds can be utilized to optimize the parameters of high-level boreholes.

4. Optimization of Goaf Gas Extraction Technology in the Production Working Face

4.1. Optimization of High-Level Directional Borehole Parameters Considering Advance Speed

According to statistical data on the gas emission and return corner gas concentration in the No. 3 mining area of the experimental mine, when the gas emission from the working face is less than $10 \text{ m}^3/\text{min}$, it can be effectively controlled below the limit through face ventilation and goaf gas extraction. During production, the gas emission from the goaf accounts for 45.5% of the total gas emission at the working face, implying that the goaf gas emission should be less than $4.55 \text{ m}^3/\text{min}$. Based on the aforementioned linear relationship between the mining speed and goaf gas emission, to ensure that working face gas emissions do not exceed the limit, the mining speed should be controlled within 8 m/d. At low mining speeds, no specific design is required. Therefore, when designing high-level gas

extraction boreholes in the goaf, the parameters should primarily focus on mining speeds of 4–8 m/d.

Based on the quantitative analysis of optimal drilling positions and spacing for a mining speed of 4–8 m per day, and taking into account the uniformity of drilling distribution, optimization and verification were conducted at the 12,302 working face of the mine. The elevation of the working face was +570~+640 m, the strike length was 2604 m, and the inclination length was 310 m. Further, the working face caving ratio was 1:1, with a bulk density of 1.44 t/m³ and a recovery ratio of 88%. It utilizes a “U”-shaped ventilation system with an average air volume of 2400 m³/min, and the coal seam gas content is 3.1 m³/t. Eight drilling sites were established in the working face. For the experimental phase, the No. 8 drilling site of the 12,302 working face was selected for optimization and verification, with five boreholes arranged at this site. The parameters of the boreholes are detailed in Table 6, and the borehole trajectories are illustrated in Figure 8.

Table 6. Drilling parameters of the No. 8 drilling site.

Drilling Site	Drilling Number	Horizontal Distance/m	Layer/m	Length/m
8#	8-1	51	43	471
	8-2	39	40	468
	8-3	30	31	465
	8-4	20	22	462
	8-5	10	10	459

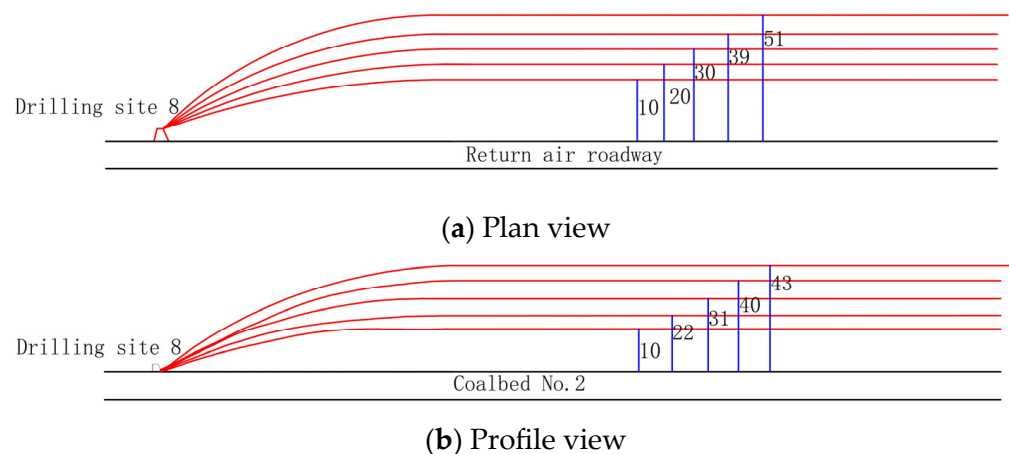


Figure 8. Schematic diagram of actual high-level drilling at a daily advancement distance of 4–8 m/d.

4.2. Investigation of Gas Extraction and Control Effectiveness

The individual borehole gas extraction volumes at drilling site No. 8 are depicted in Figure 9. As illustrated in Figure 9, the extraction volumes of each borehole group exhibit some fluctuations. The maximum gas extraction flow rate of borehole 8-1 reached 3.18 m³/min, representing a 51% increase compared to the maximum single borehole gas extraction volume at other drilling sites prior to optimization. The average gas extraction volumes for boreholes 8-1, 8-2, 8-3, 8-4, and 8-5 were 2.01, 1.55, 1.73, 0.76, and 0.68 m³/min, respectively. Compared to borehole 8-5, the extraction volumes of the other four boreholes were higher, thus verifying the rationality and feasibility of this method.

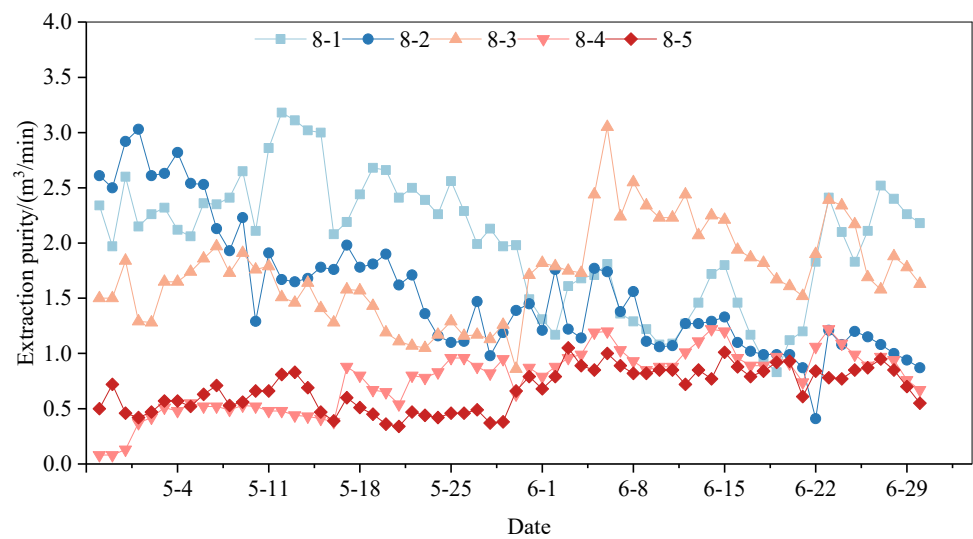


Figure 9. Variation characteristics of borehole gas extraction volume.

The daily gas extraction volumes of high-level directional boreholes, along with the gas emission volumes and gas extraction rates of the working face, are depicted in Figure 10. When the working face advance speed was below 8 m/d, the gas emission volume at the working face was generally maintained within 10 m³/min, with only five days exceeding this threshold. The average gas extraction rate of high-level directional boreholes reached 68%, with the extraction volumes of these boreholes playing a crucial role in controlling the gas emissions at the working face.

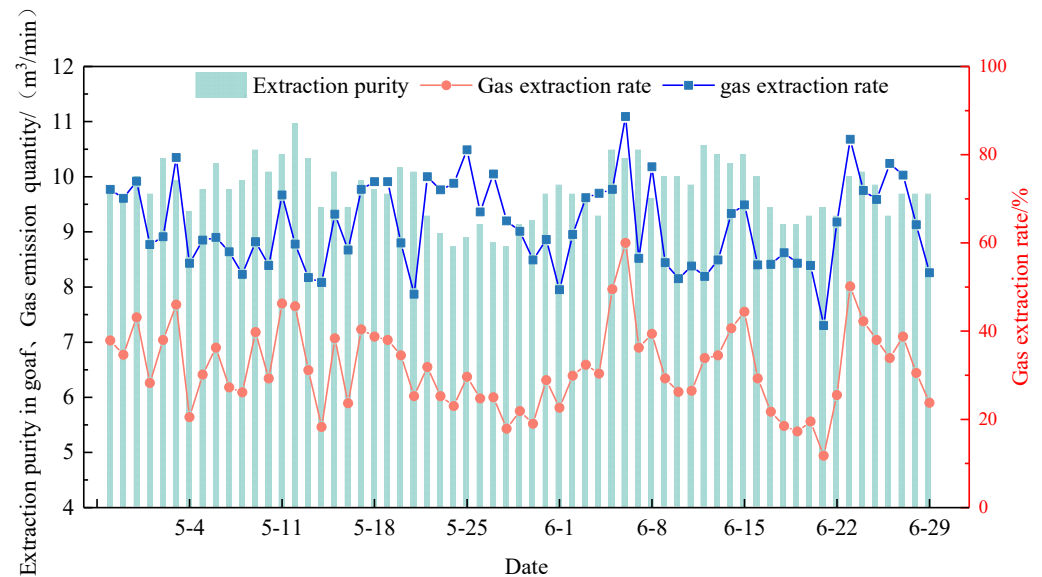


Figure 10. Variation characteristics of extraction volume, gas emission volume, and extraction rate.

The gas concentrations in the upper corner and the return airflow during the extraction period of high-level directional boreholes are illustrated in Figure 11. As illustrated in Figure 11, the maximum gas concentrations in the upper corner ranged from 0.35% to 0.7%, and the maximum gas concentrations in the return airflow ranged from 0.11% to 0.35%. Both the upper corner and return airflow gas concentrations were maintained below 0.8%, achieving the expected goal of gas control at the working face. This ensures the safe and efficient production of the mine, thus proving the feasibility of optimizing the design of high-level boreholes considering the effect of advance speed and highlighting its significant role in ensuring the safe mining of the working face.

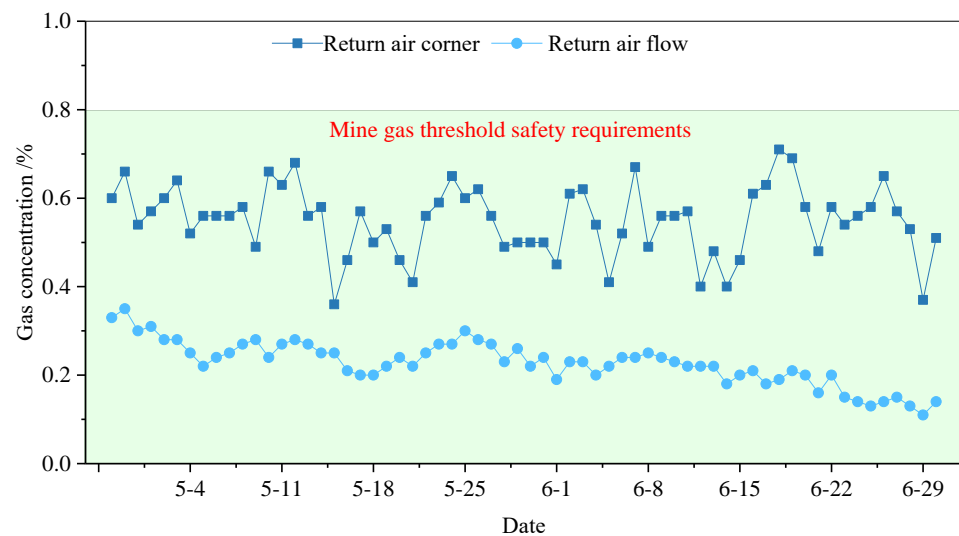


Figure 11. Variation characteristics of the gas concentration in upper corners and return airflow.

5. Discussion

“Intelligentization” and “clean low-carbon” development will be the primary directions for future mine advancements. The coal mining process is progressively entering the intelligent stage. To ensure production safety at the working face during intelligent mining, it is imperative to establish reasonable mining parameters. This study aims to offer insights and technical support for determining the mining speed and gas extraction process parameters in the intelligent mining of the working face.

This paper utilizes numerical simulation experiments and field tests to analyze the impact of the mining face speed on the development characteristics of mining-induced overburden fractures, as well as the emission and migration characteristics of gas in the goaf. Based on the results of numerical simulations and field data analysis, the influence of varying mining speeds on overburden fractures in the goaf during production and their impact on gas migration and enrichment characteristics in the goaf were determined. Furthermore, by analyzing gas enrichment characteristics, the parameters of gas extraction boreholes in the goaf were optimized, thereby improving the gas extraction capacity in the goaf.

This study primarily focuses on the impact of mining speed on the development of overburden fractures and gas migration characteristics in the goaf under fixed conditions. However, in actual mining processes, numerous factors influence mining-induced overburden fractures and gas migration characteristics in the goaf, such as variations in coal and rock properties, geological features, and gas occurrence characteristics. The impact of these factors on mining-induced overburden fractures and gas migration in the goaf requires further investigation to enhance the gas extraction capacity in the goaf.

6. Conclusions

- (1) Numerical simulations were employed to model the fracture development characteristics of the overlying strata under different working face advance speeds. The initial collapse step distance increased with the working face advance speed, whereas the maximum height of through fractures in the goaf decreased as the advance speed increased. In contrast, the development of separation fractures was primarily influenced by the advance distance of the working face and had little relationship with the advance speed.
- (2) The working face advance speed exhibits a linear correlation with gas emissions in the goaf. By categorizing and averaging gas emissions and advance speeds, the influence of factors such as the initial pressure and periodic pressure on gas emissions in the goaf can be effectively reduced, thereby increasing the correlation from 0.60 to 0.94.

The optimal drilling layer and horizontal distance of boreholes at different advance speeds also exhibit a linear relationship. As the daily advance speed increases, the slope of the line gradually decreases, while the intercept increases.

- (3) Based on the gas emission characteristics of the working face, a safe advance speed for the working face was determined. Subsequently, the parameters for high-level boreholes in the working face were optimized and applied. Consequently, the gas emission volume at the working face was effectively controlled below 10 m³/min. Throughout the entire extraction period, the average gas extraction rate of high-level directional boreholes reached 68%, and the maximum gas concentrations in the upper corner and return airflow during production remained below 0.8%.

Author Contributions: Conceptualization, C.C.; methodology, X.-Y.C.; validation, C.C., X.-Y.C. and L.C.; formal analysis, C.C.; investigation, X.-Y.C.; resources, X.-Y.C.; data curation, X.-Y.M.; writing—original draft preparation, X.-Y.C.; writing—review and editing, C.C.; visualization, C.C.; supervision, L.C.; project administration, C.C.; funding acquisition, C.C. All authors have read and agreed to the published version of the manuscript.

Funding: This research is funded by the National Key Research and Development Program of China, grant number 2023YFF0615404.

Data Availability Statement: The data used to support the findings of this study are available from the corresponding author upon request.

Conflicts of Interest: Authors Cheng Cheng, Xiao-Yu Cheng, Long Chen and Xing-Ying Ma were employed by the company China Coal Energy Research Institute Co., Ltd. They declare that the research was conducted in the absence of any commercial or financial relationships that could be construed as a potential conflict of interest. The company had no role in the design of the study; in the collection, analyses, or interpretation of data; in the writing of the manuscript, or in the decision to publish the results.

References

1. Capuano, L. *International Energy Outlook 2018 (IEO2018)*; US Energy Information Administration (EIA): Washington, DC, USA, 2018; p. 21.
2. Jiang, D.; Chen, S.; Liu, W.; Ren, Y.; Guo, P.; Li, Z. Underground hydro-pumped energy storage using coal mine goafs: System performance analysis and a case study for China. *Front. Earth Sci.* **2021**, *9*, 760464. [[CrossRef](#)]
3. Kurnia, J.C.; Sasmito, A.P.; Mujumdar, A.S. CFD simulation of methane dispersion and innovative methane management in underground mining faces. *Appl. Math. Model.* **2014**, *38*, 3467–3484. [[CrossRef](#)]
4. Zhou, W.; Yuan, L.; Zhang, G.L.; Du, H.L.; Xue, S.; He, G.H.; Han, Y.C. A new method for determining the individual sources of goaf gas emissions: A case study in Sihe Coal Mine. *J. China Coal Soc.* **2018**, *43*, 1016–1023.
5. Brodny, J.; Tutak, M. Determination of the zone endangered by methane explosion in goaf with caving of longwalls ventilated on “Y” system. *Manag. Syst. Prod. Eng.* **2016**, *24*, 247–251. [[CrossRef](#)]
6. Cheng, J.; Mei, J.; Peng, S.; Qi, C.; Shi, Y. Comprehensive consultation model for explosion risk in mine atmosphere-CCMER. *Saf. Sci.* **2019**, *120*, 798–812. [[CrossRef](#)]
7. Chen, H.; Qi, H.; Long, R.; Zhang, M. Research on 10-year tendency of China coal mine accidents and the characteristics of human factors. *Saf. Sci.* **2012**, *50*, 745–750. [[CrossRef](#)]
8. Yu, X.; Gao, M.; Zhao, H.; Zhao, S.; Zhao, H. Research on the Laws of Overlying Rock Fracture and Energy Release under Different Mining Speeds. *Appl. Sci.* **2024**, *14*, 3222. [[CrossRef](#)]
9. Whittles, D.N.; Lowndes, I.S.; Kingman, S.W.; Yates, C.; Jobling, S. Influence of geotechnical factors on gas flow experienced in a UK longwall coal mine panel. *Int. J. Rock Mech. Min. Sci.* **2006**, *43*, 369–387. [[CrossRef](#)]
10. Raabe, D. The materials science behind sustainable metals and alloys. *Chem. Rev.* **2023**, *123*, 2436–2608. [[CrossRef](#)]
11. Yang, M.; Guo, L.; Wu, X.; Li, N.; Li, X.; Zhang, N. Subpore-mediated tunable water absorption in nanoparticle-based materials. *Int. J. Heat Mass Transf.* **2024**, *231*, 125811. [[CrossRef](#)]
12. Wang, L.; Wang, Z.; Xu, S.; Zhou, W.; Wu, J. A field investigation of the deformation of protected coal and its application for CBM extraction in the Qinglong coalmine in China. *J. Nat. Gas Sci. Eng.* **2015**, *27*, 367–373. [[CrossRef](#)]
13. Bondarev, A.; Mihai, S.; Pântea, O.; Neagoe, S. Use of biopolymers for the removal of metal ion contaminants from water. In *Macromolecular Symposia*; WILEY-VCH: Weinheim, Germany, 2011; Volume 303, pp. 78–84.
14. Qian, M.G.; Xu, J.L. Study on the “O-shape” circle distribution characteristics of mining induced fractures in the overlying strata. *J. China Coal Soc.* **1998**, *23*, 466–469.

15. Yuan, L.; Guo, H.; Shen, B.T.; Qu, Q.D.; Xue, J.H. Circular overlying zone at longwall panel for efficient methane capture of multiple coal seams with low permeability. *J. China Coal Soc.* **2011**, *36*, 357–365.
16. Li, S.G.; Shi, P.W.; Qian, M.G. Study on the dynamic distribution features of mining fissure elliptic paraboloid zone. *Ground Press. Strat. Control* **1999**, *3*, 44–46.
17. Islam, M.R.; Hayashi, D.; Kamruzzaman, A.B.M. Finite element modeling of stress distributions and problems for multi-slice longwall mining in Bangladesh, with special reference to the Barapukuria coal mine. *Int. J. Coal Geol.* **2009**, *78*, 91–109. [[CrossRef](#)]
18. Wu, W.D.; Bai, J.B.; Wang, X.Y.; Yan, S.; Wu, S.X. Numerical study of failure mechanisms and control techniques for a gob-side yield pillar in the Sijiazhuang coal mine, China. *Rock Mech. Rock Eng.* **2019**, *52*, 1231–1245. [[CrossRef](#)]
19. Lin, H.F.; Li, S.G.; Cheng, L.H.; Wang, H.S. Experimental analysis of dynamic evolution model of mining-induced fissure zone in overlying strata. *J. Min. Saf. Eng.* **2011**, *28*, 298–303.
20. Yujun, Z.; Huaxing, Z.; Peipei, C. Visual exploration of fissure field of overburden and rock. *J. China Coal Soc.* **2008**, *33*, 1216–1219.
21. Kang, Y.; Wang, J.; Kong, F.; Liu, X.E.; Jin, R.C.; Zheng, J.Q. Bore hole survey method for overburden failure. *Coal Sci. Technol.* **2002**, *30*, 26–28.
22. Yang, Y.; Liang, P. The detection technology of goaf overburden rock damage of based on EH4 electromagnetic imaging system. *Chin. J. Geol. Hazard. Control* **2013**, *24*, 68–71.
23. Zhang, H.W.; Zhu, Z.J.; Huo, L.J.; Chen, Y.; Huo, B.J. Overburden failure height of superhigh seam by fully mechanized caving method. *J. China Coal Soc.* **2014**, *39*, 816–821.
24. Zhou, H.; Liu, J.; Xue, D.; Yi, H.; Xue, J. Numerical simulation of gas flow process in mining-induced crack network. *Int. J. Min. Sci. Technol.* **2012**, *22*, 793–799. [[CrossRef](#)]
25. Qin, Z.; Yuan, L.; Guo, H.; Qu, Q. Investigation of longwall goaf gas flows and borehole drainage performance by CFD simulation. *Int. J. Coal Geol.* **2015**, *150*, 51–63. [[CrossRef](#)]
26. Guo, H.; Yuan, L.; Shen, B.; Qu, Q.; Xue, J. Mining-induced strata stress changes, fractures and gas flow dynamics in multi-seam longwall mining. *Int. J. Rock Mech. Min. Sci.* **2012**, *54*, 129–139. [[CrossRef](#)]
27. Zhang, C.; Chen, Y.; Ren, Z.; Wang, F. Compaction and seepage characteristics of broken coal and rock masses in coal mining: A review in laboratory tests. *Rock Mech. Bull.* **2024**, *3*, 100102. [[CrossRef](#)]
28. Liu, Y.; Shao, S.; Wang, X.; Chang, L.; Cui, G.; Zhou, F. Gas flow analysis for the impact of gob gas ventholes on coalbed methane drainage from a longwall gob. *J. Nat. Gas Sci. Eng.* **2016**, *36*, 1312–1325. [[CrossRef](#)]

Disclaimer/Publisher’s Note: The statements, opinions and data contained in all publications are solely those of the individual author(s) and contributor(s) and not of MDPI and/or the editor(s). MDPI and/or the editor(s) disclaim responsibility for any injury to people or property resulting from any ideas, methods, instructions or products referred to in the content.